**Showcasing work from the groups of
Dr Valentin A. Milichko, School of Physics and Engineering,
ITMO University, Russia, and Professor Thierry Belmonte,
Institut Jean Lamour, Université de Lorraine, France.**

FeAu mixing for high-temperature control of light scattering
at the nanometer scale

Mixing of weakly miscible elements inside the NP supports a
thermal-induced phase transformation from a homogeneous
metastable solid solution phase into biphasic Janus-type NP,
resulting in optical tuning triggered by a high temperature.
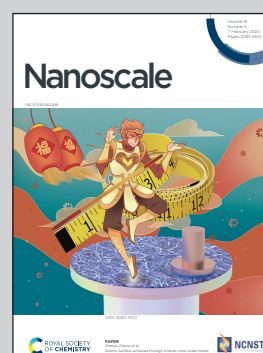
ROYAL SOCIETY
OF **CHEMISTRY**

rsc.li/nanoscale

Check for updates

FeAu mixing for high-temperature control of light scattering at the nanometer scale†

Anna V. Nominé, [ID] ‡[a] Ekaterina V. Gunina,‡[b] Semyon V. Bachinin,[b]
Alexander I. Solomonov, [ID] [b] Mikhail V. Rybin,[b,c] Sergei A. Shipilovskikh, [ID] [b]
Salah-Eddine Benrazzouq, [ID] [a] Jaafar Ghanbaja,[a] Thomas Gries,[a] Stephanie Bruyère,[a]
Alexandre Nominé,[a,d,e] Thierry Belmonte*[a] and Valentin A. Milichko [ID] *[a,b]

Control of the optical properties of a nanoparticle (NP) through its structural changes underlies optical data processing, dynamic coloring, and smart sensing at the nanometer scale. Here, we report on the concept of controlling the light scattering by a NP through mixing of weakly miscible chemical elements (Fe and Au), supporting a thermal-induced phase transformation. The transformation corresponds to the transition from a homogeneous metastable solid solution phase of the (Fe,Au) NP towards an equilibrium biphasic Janus-type NP. We demonstrate that the phase transformation is thermally activated by laser heating up to a threshold of 800 °C (for NPs with a size of hundreds of nm), leading to the associated changes in the light scattering and color of the NP. The results thereby pave the way for the implementation of optical sensors triggered by a high temperature at the nanometer scale *via* NPs based on metal alloys.

Nanoparticles (NPs) have emerged as an important class of nanomaterials for optical application due to their unique properties, arising from their small size and high surface-to-volume ratio, which are not characteristic of their bulk counterparts. Localized surface plasmon resonances and strong light scattering allow enhanced light absorption or electromagnetic field confinement/redirection for imaging, sensing, and efficient energy conversion.[1–3] In the preliminary stage, the optical properties of NPs can be easily tuned during their synthesis allowing one to control their size, shape, and composition.[4] As a result, such versatility has made them attractive for diverse applications (such as biomedical imaging, photocatalysis, drug delivery, and optical data storage).[5–8]

Next, tuning the optical properties of NPs of a fixed size, shape, and composition extends the application of NPs for optical data processing, dynamic colouring, and smart sensing[9–14] due to the dynamic changes in their structure-related optical properties under the action of external stimuli. This approach became possible to implement through the use of adaptive complex materials, which react structurally or electronically to external optical, electronic or chemical stimuli.[15,16] To date, the control of the NP structure through phase transitions remains one of the most efficient approaches to precisely control the NP optical properties.[17–23] However, this approach is still in its infancy due to the limited list of materials and structures undergoing effective phase transformations at the nanometer scale and allowing simultaneously sustainable green tech transition in micro- and optoelectronics.[24]

Here, we report on the concept of mixing weakly miscible chemical elements (Fe and Au) *via* laser ablation to produce metal alloy NPs possessing the ability to undergo phase transformation at a specific temperature. The transformation corresponds to a phase transition from a homogeneous metastable solid solution phase of the (Fe,Au) NP towards an equilibrium biphasic Janus-type NP. We also demonstrate that the transformation is thermally activated by laser heating up to a threshold of 800 °C (for NPs with a size of hundreds of nm). As a result, one can observe the associated changes in the light scattering and colour of the NPs. The results thereby pave the way for the implementation of optical high-temperature triggers at the nanometer scale *via* NPs based on metal alloys.

In the first stage, we screened weakly miscible elements: among the numerous possibilities, Au and Fe are of great interest from the fundamental point of view due to their extended miscibility gaps and deviating crystal structures (Fig. 1c). Indeed, Au has a face-centred cubic (fcc) structure, while Fe demonstrates either a body-centred cubic (bcc) or an fcc structure. Among the commonly encountered structures,

[a]Institut Jean Lamour, Université de Lorraine, UMR CNRS 7198, 54011 Nancy, France. E-mail: valentin.milichko@univ-lorraine.fr, thierry.belmonte@univ-lorraine.fr
[b]School of Physics and Engineering, ITMO University, St. Petersburg, 197101, Russia
[c]Ioffe Institute, St. Petersburg 194021, Russia
[d]LORIA, University of Lorraine – INRIA - CNRS, Vandoeuvre lès Nancy, France
[e]Department of Gaseous Electronics, Jožef Stefan Institute, Ljubljana, Slovenia
†Electronic supplementary information (ESI) available. See DOI: https://doi.org/10.1039/d3nr05117j
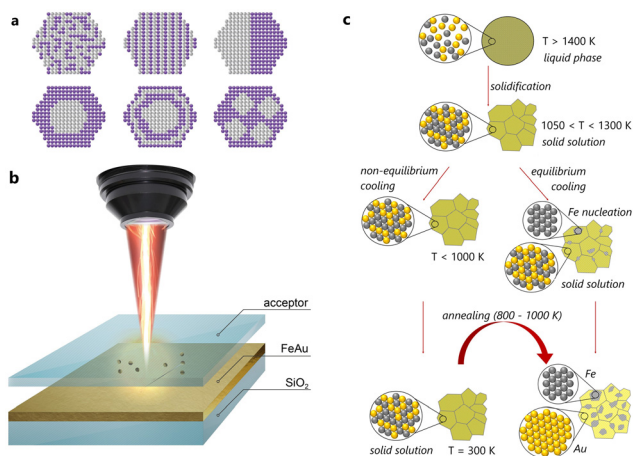‡ Equal contribution.

Fig. 1 (a) Types of bimetallic NPs with different distributions of elements over the NP volume, including an alloy state, which can be obtained by various physicochemical methods such as laser ablation (b). (c) Scheme of (Fe,Au) NP transformation.

formed from liquid droplets made of Au and Fe, one finds alloy NPs with a disordered solid solution mixture, core–shell NPs with an Fe core and an Au shell, as well as nested core–shell NPs with multiple cores.[25] The final internal phase structure (also named "ultrastructure") of (Fe,Au) NPs is strongly affected by their composition and diameter.[26–30] In detail, Kamp *et al.* reported[27] that the metastable spherical core–shell $Fe_{80}Au_{20}$ NPs overcame the transformation to Janus-type or cube-shaped Fe-rich core NPs with Au-rich pyramids by heating up to 700 °C. However, for $Fe_{50}Au_{50}$ NPs, the Au-rich shell solved into the Fe-rich core, and solid solution NPs formed *via* an intermediate lamellar ultrastructure. In contrast, in the segregated structures, Au and Fe nanodomains of 5–10 nm size can be distinguished easily. Moreover, Fe and Au exhibit limited solubility at room temperature (around 2 wt% of Fe in Au and a fraction of wt% of Au in Fe), while at elevated temperatures, miscibility can be achieved (~24 wt% of Fe in Au and about 4 wt% of Au in Fe at 877 °C). Depending on the temperature (Fig. S1†), these elements might be mixed within a single solid solution up to a concentration of 74 at% of Fe at a temperature of 1027 °C, corresponding to the peritectic point. This is presumably a favourable condition to stabilize the solid solution at a temperature lower than the solubility limit.

Based on this, we have fabricated thin films by simultaneous physical vapour deposition (PVD) of Fe and Au on silica (see the ESI†). The resulting (Fe,Au) films with 660 ± 40 nm thicknesses and closer to equimolar composition (56 at% of Au and 44 at% of Fe, Fig. S3, S4 and Table S1†) have been then subjected to laser ablation in gases to obtain the corresponding NPs (for experimental details, see the ESI†). First, this process allows easy fabrication of multicomponent alloys *via* non-equilibrium heating and cooling (Fig. 1b).[31–38] Second, the laser ablation in gases is related to the possibility of controlling their size distribution[39] and the position of each

synthesized NP on the substrate for precise measurement of their optical properties.[40] For the gas atmosphere, we used air and N_2 to tune the composition, morphology, and optical properties of the resulting NPs (see below).

Then, the NPs obtained were analysed by transmission electron microscopy (TEM) and elemental analysis. Fig. 2 shows that the resulting NPs possess a spherical shape with diameters from 10 to 300 nm (extended, with rare exceptions, up to 600 nm, Fig. S8†). Herein, energy-dispersive X-ray (EDX) analysis (Fig. 2e and k) revealed that the NPs obtained by laser ablation in air contain 36 at% of O, 14 at% of Fe and 50 at% of Au (Table S1†), while the NPs obtained by laser ablation in N_2 contain only 13 at% of O, 30 at% of Fe and 57 at% of Au (Table S2†). Elemental analysis also showed that the NPs obtained in air demonstrate a core–shell structure with a high concentration of Au in the core (Fig. 2g–l), while the NPs obtained under an N_2 atmosphere possess a uniform distribution of Fe and Au elements over the NP volume (Fig. 2a–f). Moreover, high-resolution TEM revealed the high level of crystallinity of the NPs, obtained under air (Fig. S10†) and N_2 (Fig. S11†), and confirmed that they exhibit the same features as those described by Kamp *et al.*[27,28] Based on these results, we focus mostly on N_2-produced NPs in order to stay closer to the composition of the initial (Fe,Au) film. The size distribution of such NPs (from 10 to 600 nm) is also presented in Fig. S9.†

Next, to show experimentally the energetically favourable process of separation of Fe and Au inside the NPs (Fig. 1c) and its effect on their optical properties, we heated single NPs with laser radiation. For that, we chose an effective absorption wavelength for Fe and Au (350 nm) and analysed simultaneously the light scattering by a single NP in dark field geometry[41–44] before and during the laser heating (see the ESI†). Fig. 3a shows that the N_2-produced NP with an average size of 200 ± 50 nm before the heating exhibits broad peaks of light scatter-

Fig. 2 Bright field scanning TEM (STEM) micrographs of the NPs obtained by laser ablation of the (Fe,Au) film under an N_2 (a−d) and air (g−j) atmosphere, respectively; (e and k) bidimensional EDX spectroscopy maps of the selected NPs obtained under an N_2 and air atmosphere, respectively, and (f and l) their EDX elemental line scan analysis.
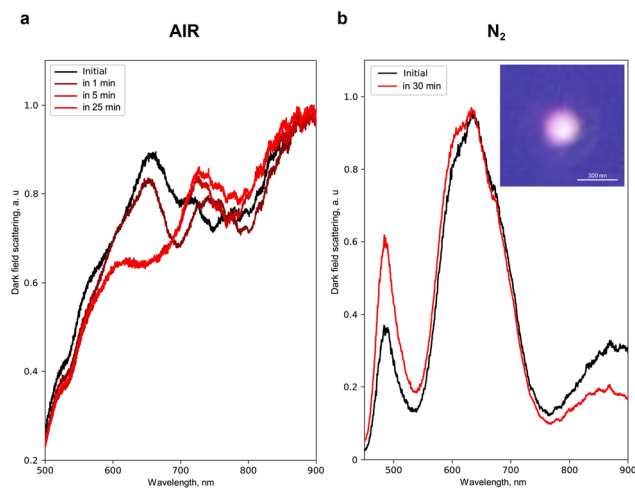
Fig. 3 Dark field scattering spectra of single N_2-produced NPs (200 $\pm$ 50 nm in diameter) upon laser heating under an air (a) and N_2 (b) atmosphere, respectively, with the corresponding optical image of the NP before heating under an N_2 atmosphere (inset).

Fig. 4 (a–c) High-angle annular dark-field (HAADF) STEM micrographs and EDX analysis of *in situ* heated N_2-produced NPs in a TEM chamber from room temperature (a) up to 800 °C (b). (d) HAADF STEM micrograph of the obtained Janus-type (Fe,Au) NP. (e) Scattering cross-section of the NP before (black curve) and after laser heating (red curve) with the corresponding decomposition of electromagnetic modes (f). (g) Electric field distribution (at wavelengths of 593 nm (bottom), 700 nm (middle), and 907 nm (top)) for a single NP after heating.

ing at 650 and 900 nm. However, upon heating in air, a new peak centred at 750 nm appears in 1 min followed by a 30–50 nm blue shift of 650 and 750 nm peaks (during 5 to 30 min of continuous heating). Herein, a 950 nm peak remains unchanged. A similar spectrum of light scattering is obtained for the N_2-produced NPs with an average size of 200 $\pm$ 50 nm heated under an N_2 atmosphere (Fig. 3b): broad peaks centred at 650 and 900 nm, as well as a narrow one at 500 nm. Upon heating under N_2, these peaks also demonstrate a blue shift by 2–5 nm, thereby eliminating the negative effect of Fe oxidation on the spectral changes. The latter is also supported by the fact that laser heating for more than 25 min supports no changes in the light scattering for N_2-produced NPs, while the potential oxidation process of 30% Fe inside these NPs should lead to more sufficient and continuous spectral changes upon continuous laser heating.[45] Statistical analysis[46] of the effect of heating on the change of the light scattering spectrum for NPs of different sizes and arbitrary element concentrations is also presented in Fig. S20.†

To shed light on the mechanism of transformation of the NPs[33–38] and accompanying optical changes during the laser heating, we performed *in situ* TEM analysis in the heating mode. As one can see in Fig. 4a–c and S12–14,† the heating of spherical homogeneous NPs (produced under an N_2 atmosphere) to a temperature of 800 $\pm$ 100 °C (depending on the Fe/Au ratio and the NP size) leads to a separation of elements over the NP volume.[33–38] Herein, the initial spherical shape and the Fe/Au ratio remain unchanged. Indeed, if the transformation from a metastable solid solution to a biphasic system is thermodynamically favourable, such diffusive transformation should be time- and temperature-dependent. This is why such transformation is faster to observe at higher temperature. However, this temperature should be as close as possible to the solubility limit (*e.g.* 875 °C for an equimolar (Fe,Au)
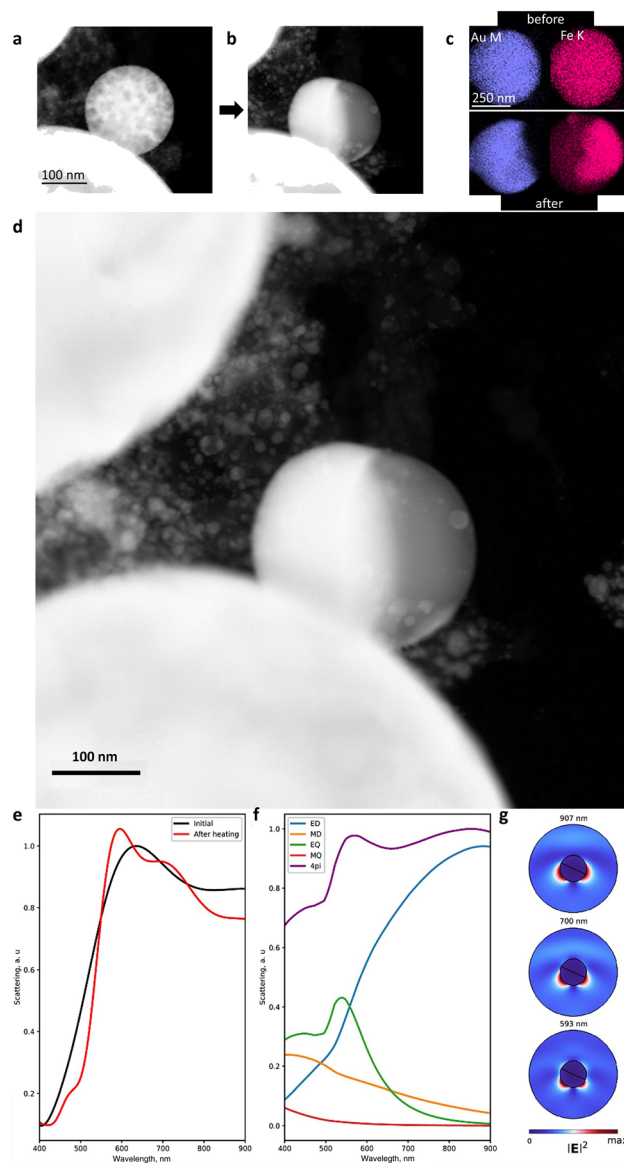
system under ambient conditions, Fig. S1†). The results obtained confirm that varying the Fe/Au ratio provides smooth control of the separation temperature, thereby opening up the possibility of creating optical triggers controlled by extreme temperatures. Intriguingly, according to the phase diagram (Fig. S1†), it should be theoretically possible to realize the reverse transformation (from a Janus-type to a homogeneous metastable solid solution phase) provided that the temperature is sufficiently high. However, the cooling would have to be extremely fast to stabilize the phase. Moreover, the heating

would have to be at a sufficiently high temperature to trigger the transformation, but not so high to avoid transition to a liquid. The latter implies dewetting and a strong modification of the NP shape (from spherical to hemispherical). In addition, we have analyzed the dependence of the transformation temperature on the NP size (Fig. S15†) and revealed that an increase in the NP size (from 10 to 600 nm) yields an increase in the transition temperature from 400 to 800 °C (with 100 °C error). However, due to the diffusive nature of the transformation, its observation is also possible over time at low temperatures.

Taking these results into account and considering the differences in melting and dew points of Fe and Au, we performed the numerical simulation of the light scattering by such NPs before and after their transformation (Fig. 4e–g). For this, we considered a 300 nm spherical NP as a model with a homogeneous Fe and Au distribution (Fig. S16a†), excited with a linearly p-polarized white light at an angle of 65° to the pole axis of the NP.[47] Then, we integrated the scattering light in a 0.7π solid angle corresponding to a 0.42 numerical aperture of the objective (see the ESI†). We also proposed that cubic domains of Au and Fe of 10 nm size formed upon heating, followed by domain wall growth, leading to more pronounced separation of Fe and Au.[33–38] In the final stage of heating, complete separation of Fe and Au happened inside the NP with the appearance of two hemispheres (Fig. 4b, d and S16c†). The corresponding spectra of light scattering by the NP before the laser heating are shown in Fig. 4e: two broad peaks are observed at 630 nm and 920 nm, in good agreement with the experimental results (Fig. 3a and b). To determine the origin of these peaks, we applied Mie theory with an averaged permittivity, using the effective medium theory:[48] an effective permittivity ε_{eff} of the NP before heating has been calculated using the Lorentz–Lorenz relation $(\varepsilon_{eff} - 1)/(\varepsilon_{eff} + 2) = \delta(\varepsilon_{Au} - 1)/(\varepsilon_{Au} + 2) + (1 - \delta)(\varepsilon_{Fe} - 1)/(\varepsilon_{Fe} + 2)$, where δ is the fraction of Au in the NP ranging from 0 to 1 and ε_{Au} and ε_{Fe} are the complex permittivity of Au and Fe, respectively. Based on this, we attributed the 920 nm peak in Fig. 4e to the broadband surface plasmon resonance with an electric dipole (ED) field profile, while the 630 nm peak corresponds to the surface plasmon resonance with an electric quadrupole (EQ) field profile combined with an ED (Fig. 4f). Herein, magnetic dipole and quadrupole (MD and MQ) make a negligible contribution to light scattering efficiency. However, after the heating, the calculation determined the scattering resonances at 593 nm, 700 nm, and 907 nm (Fig. 4e). The multipole expansion revealed their origin (Fig. 4g):[49] the peak centred at 907 nm corresponds to a surface plasmon resonance with an ED field profile (as for the 920 nm peak of the NP before heating) and the 700 nm peak corresponds to the same localized plasmon resonance combined with the EQ mode, while the 593 nm peak corresponds to a localized plasmon resonance with the EQ field profile combined with electric and magnetic dipole modes (ED and MD). The latter indicates that the laser heating initiates a 20–40 nm blue shift for the light scattering, which is in good agreement with the experimental data in Fig. 3a and

b. In addition, we numerically investigated the effect of the uncertain orientation of the Janus-type (Fe,Au) NPs relative to the incident light on their scattering spectra (Fig. S18 and S19†).[50] As one can see, an arbitrary position of such NPs demonstrates negligible impact on the spectral position of the scattering resonances, as well as the total scattering spectrum.

Finally, the calculated data qualitatively describe the experimental evolution of the light scattering by the NP during the laser heating. This supports the proposed concept of energetically favourable separation of the weakly miscible elements leading to the change in the optical properties of the corresponding NP. However, since the element separation process requires some energy, it appeared to be a threshold effect, which opens up great prospects for the use of such NPs as optical sensors[51,52] at the nanometre scale, triggered by specific extreme temperatures (depending on the element ratio). In addition, due to the wide list of immiscible (or weakly miscible) elements such as Fe and Au, Au and Cu, Cu and W, Cu and Ag, Al and Zn, and Pb and Sn, the chemical composition of the NPs can be varied, which also provides (besides the varied ratio of elements) an opportunity to tune the threshold temperature initiating the NP transformation.

Conclusions

In summary, we report on a new concept of controlling the optical properties of a single NP through the mixing of weakly miscible elements such as Fe and Au, supporting a phase transformation at a precise given temperature. Such transformation corresponds to a phase transition from a homogeneous metastable solid solution phase of the NP containing Fe and Au towards an equilibrium biphasic system with pure Fe and Au forming a Janus-type NP. We reveal that the transformation can be thermally activated by laser heating up to 800 °C, leading to the associated changes of optical scattering of the NPs, confirmed numerically and experimentally. The results pave the way for the implementation of optical high-temperature triggers at the nanometer scale via NPs based on weakly miscible alloys.

Author contributions

V. A. M. and T. B. conceptualised the study. A. V. N. and E. V. G. obtained the thin films and NPs and contributed to TEM and optical experiments, as well as the data analysis. S. E. B. contributed to PVD thin film fabrication. S. V. B. contributed to the optical experiments. A. I. S. and M. V. R. performed the calculations. J. G. and S. B. performed TEM elemental analysis. T. G. contributed to film fabrication and SEM experiments. S. A. S. discussed the structural data. A. N., T. B. and V. A. M. contributed to data analysis, discussion and paper writing.

Conflicts of interest

There are no conflicts to declare.

Acknowledgements

References

1 O. Nicoletti, F. de la Peña, R. K. Leary, D. J. Holland, C. Ducati and P. A. Midgley, *Nature*, 2013, **502**, 80–84.

2 W. P. Putnam, R. G. Hobbs, P. D. Keathley, K. K. Berggren and F. X. Kärtner, *Nat. Phys.*, 2017, **13**, 335–339.

3 E. Cortés, W. Xie, J. Cambiasso, A. S. Jermyn, R. Sundararaman, P. Narang, S. Schlücker and S. A. Maier, *Nat. Commun.*, 2017, **8**, 14880.

4 I. Lisiecki, *J. Phys. Chem. B*, 2005, **109**, 12231–12244.

5 O. S. Wolfbeis, *Chem. Soc. Rev.*, 2015, **44**, 4743–4768.

6 C. Xu, P. R. Anusuyadevi, C. Aymonier, R. Luque and S. Marre, *Chem. Soc. Rev.*, 2019, **48**, 3868–3902.

7 M. J. Mitchell, M. M. Billingsley, R. M. Haley, M. E. Wechsler, N. A. Peppas and R. Langer, *Nat. Rev. Drug Discovery*, 2021, **20**, 101–124.

8 M. Gu, Q. Zhang and S. Lamon, *Nat. Rev. Mater.*, 2016, **1**, 16070.

9 M. R. Shcherbakov, S. Liu, V. V. Zubyuk, A. Vaskin, P. P. Vabishchevich, G. Keeler, T. Pertsch, T. V. Dolgova, I. Staude, I. Brener and A. A. Fedyanin, *Nat. Commun.*, 2017, **8**, 17.

10 X. Liu, *Front. Mater.*, 2018, **5**, 59.

11 A. Kristensen, J. K. W. Yang, S. I. Bozhevolnyi, S. Link, P. Nordlander, N. J. Halas and N. A. Mortensen, *Nat. Rev. Mater.*, 2017, **2**, 16088.

12 M. Elbahri, S. Homaeigohar and M. A. Assad, *Adv. Photonics Res.*, 2021, **2**, 2100009.

13 R. Feng, H. Wang, Y. Cao, Y. Zhang, R. J. H. Ng, Y. S. Tan, F. Sun, C.-W. Qiu, J. K. W. Yang and W. Ding, *Adv. Funct. Mater.*, 2022, **32**, 2108437.

14 M. Segev-Bar, A. Landman, M. Nir-Shapira, G. Shuster and H. Haick, *ACS Appl. Mater. Interfaces*, 2013, **5**, 5531–5541.

15 P. Talianov, L. I. Fatkhutdinova, A. S. Timin, V. A. Milichko and M. V. Zyuzin, *Laser Photonics Rev.*, 2021, **15**, 2000421.

16 N. Kulachenkov, M. Barsukova, P. Alekseevskiy, A. A. Sapianik, M. Sergeev, A. Yankin, A. A. Krasilin, S. Bachinin, S. Shipilovskikh, P. Poturaev, N. Medvedeva, E. Denislamova,

17 Y. Chen, Z. Lai, X. Zhang, Z. Fan, Q. He, C. Tan and H. Zhang, *Nat. Rev. Chem.*, 2020, **4**, 243–256.

18 Y. Wang, P. Landreman, D. Schoen, K. Okabe, A. Marshall, U. Celano, H.-S. P. Wong, J. Park and M. L. Brongersma, *Nat. Nanotechnol.*, 2021, **16**, 667–672.

19 B. Chen, G. H. ten Brink, G. Palasantzas and B. J. Kooi, *Sci. Rep.*, 2016, **6**, 39546.

20 M. Rudé, V. Mkhitaryan, A. E. Cetin, T. A. Miller, A. Carrilero, S. Wall, F. J. G. de Abajo, H. Altug and V. Pruneri, *Adv. Opt. Mater.*, 2016, **4**, 1060–1066.

21 D. Kumaar, M. Can, K. Portner, H. Weigand, O. Yarema, S. Wintersteller, F. Schenk, D. Boskovic, N. Pharizat, R. Meinert, E. Gilshtein, Y. Romanyuk, A. Karvounis, R. Grange, A. Emboras, V. Wood and M. Yarema, *ACS Nano*, 2023, **17**, 6985–6997.

22 S. Lepeshov, A. Krasnok and A. Alù, *ACS Photonics*, 2019, **6**, 2126–2132.

23 M. Wuttig, H. Bhaskaran and T. Taubner, *Nat. Photonics*, 2017, **11**, 465–476.

24 N. Kulachenkov, Q. Haar, S. Shipilovskikh, A. Yankin, J.-F. Pierson, A. Nominé and V. A. Milichko, *Adv. Funct. Mater.*, 2022, **32**, 2107949.

25 C. Zelenka, M. Kamp, K. Strohm, A. Kadoura, J. Johny, R. Koch and L. Kienle, *arXiv*, 2022, preprint, arXiv: 2207.14023, DOI: **10.48550/arXiv.2207.14023**.

26 M. N. Magomedov, *Solid State Sci.*, 2021, **120**, 106721.

27 M. Kamp, A. Tymoczko, U. Schürmann, J. Jakobi, C. Rehbock, K. Rätzke, S. Barcikowski and L. Kienle, *Cryst. Growth Des.*, 2018, **18**, 5434–5440.

28 M. Kamp, A. Tymoczko, R. Popescu, U. Schürmann, R. Nadarajah, B. Gökce, C. Rehbock, D. Gerthsen, S. Barcikowski and L. Kienle, *Nanoscale Adv.*, 2020, **2**, 3912–3920.

29 J. Johny, O. Prymak, M. Kamp, F. Calvo, S. H. Kim, A. Tymoczko, A. El-Zoka, C. Rehbock, U. Schürmann, B. Gault, L. Kienle and S. Barcikowski, *Nano Res.*, 2022, **15**, 581–592.

30 A. Tymoczko, M. Kamp, O. Prymak, C. Rehbock, J. Jakobi, U. Schürmann, L. Kienle and S. Barcikowski, *Nanoscale*, 2018, **10**, 16434–16437.

31 V. Amendola, S. Scaramuzza, F. Carraro and E. Cattaruzza, *J. Colloid Interface Sci.*, 2017, **489**, 18–27.

32 Z. Lin, J. Yue, L. Liang, B. Tang, B. Liu, L. Ren, Y. Li and L. Jiang, *Appl. Surf. Sci.*, 2020, **504**, 144461.

33 A. Tymoczko, M. Kamp, O. Prymak, C. Rehbock, J. Jakobi, U. Schürmann, L. Kienleb and S. Barcikowski, *Nanoscale*, 2018, **10**, 16434–16437.

34 M. V. Efremova, M. Spasova, M. Heidelmann, I. S. Grebennikov, Z. Li, A. S. Garanina, I. O. Tcareva, A. S. Savchenko, M. Farle, N. L. Klyachko, A. G. Majouga and U. Wiedwald, *Nanoscale*, 2021, **13**, 10402.

35 V. Amendola, S. Scaramuzza, F. Carraro and E. Cattaruzza, *J. Colloid Interface Sci.*, 2017, **489**, 18–27.

36 M. Kamp, A. Tymoczko, R. Popescu, U. Schürmann, R. Nadarajah, B. Gökce, C. Rehbock, D. Gerthsen, S. Barcikowski and L. Kienle, *Nanoscale Adv.*, 2020, **2**, 3912–3920.

37 J. Vernieres, S. Steinhauer, J. Zhao, A. Chapelle, P. Menini, N. Dufour, R. E. Diaz, K. Nordlund, F. Djurabekova, P. Grammatikopoulos and M. Sowwan, *Adv. Funct. Mater.*, 2017, 1605328.

38 I. A. Zhuravlev, S. V. Barabash, J. M. An and K. D. Belashchenko, *Phys. Rev. B*, 2017, **96**, 134109.

39 M. Karsakova, N. Shchedrina, A. Karamyants, E. Ponkratova, G. Odintsova and D. Zuev, *Langmuir*, 2023, **39**, 204–210.

40 U. Zywietz, A. B. Evlyukhin, C. Reinhardt and B. N. Chichkov, *Nat. Commun.*, 2014, **5**, 3402.

41 P. A. Dmitriev, S. V. Makarov, V. A. Milichko, I. S. Mukhin, A. S. Gudovskikh, A. A. Sitnikova, A. K. Samusev, A. E. Krasnok and P. A. Belov, *Nanoscale*, 2016, **8**, 5043–5048.

42 L. R. Mingabudinova, A. S. Zalogina, A. A. Krasilin, M. I. Petrova, P. Trofimov, Y. A. Mezenov, E. V. Ubyivovk, P. Lönnecke, A. Nominé, J. Ghanbaja, T. Belmonte and V. A. Milichko, *Nanoscale*, 2019, **11**, 10155–10159.

43 L.-E. Bataille, I. S. Merenkov, V. V. Yaroshenko, P. N. Kustov, P. V. Alekseevskiy, N. K. Kulachenkov, Y. Kenzhebayeva, A. A. Krasilin, R. Savelev, D. Zuev, A. Nominé, J. Zollinger, A. A. Voroshnina, M. L. Kosinova and V. A. Milichko, *ACS Appl. Nano Mater.*, 2022, **5**, 6106–6114.

44 N. K. Kulachenkov, S. Bruyere, S. A. Sapchenko, Y. A. Mezenov, D. Sun, A. A. Krasilin, A. Nominé, J. Ghanbaja, T. Belmonte, V. P. Fedin, E. A. Pidko and V. A. Milichko, *Adv. Funct. Mater.*, 2020, **30**, 1908292.

45 Q. Li and R. Jin, *Nanotechnol. Rev.*, 2017, **6**, 601–612.

46 R. E. Noskov, A. Machnev, I. I. Shishkin, M. V. Novoselova, A. V. Gayer, A. A. Ezhov, E. A. Shirshin, S. V. German, I. D. Rukhlenko, S. Fleming, B. N. Khlebtsov, D. A. Gorin and P. Ginzburg, *Adv. Mater.*, 2021, **33**, 2008484.

47 Y. Kenzhebayeva, S. Bachinin, A. I. Solomonov, V. Gilemkhanova, S. A. Shipilovskikh, N. Kulachenkov, S. P. Fisenko, M. V. Rybin and V. A. Milichko, *J. Phys. Chem. Lett.*, 2022, **13**, 777–783.

48 C. H. Chu, M. L. Tseng, J. Chen, P. C. Wu, Y.-H. Chen, H.-C. Wang, T.-Y. Chen, W. T. Hsieh, H. J. Wu, G. Sun and D. P. Tsai, *Laser Photonics Rev.*, 2016, **10**, 1600106.

49 K. V. Baryshnikova, D. A. Smirnova, B. S. Luk'yanchuk and Y. S. Kivshar, *Adv. Opt. Mater.*, 2019, **7**, 1801350.

50 H. Barhom, A. A. Machnev, R. E. Noskov, A. Goncharenko, E. A. Gurvitz, A. S. Timin, V. A. Shkoldin, S. V. Koniakhin, O. Y. Koval, M. V. Zyuzin, A. S. Shalin, I. I. Shishkin and P. Ginzburg, *Nano Lett.*, 2019, **19**, 7062–7071.

51 G.-Q. Liu, X. Feng, N. Wang, Q. Li and R.-B. Liu, *Nat. Commun.*, 2019, **10**, 1344.

52 S. Ma, Y. Xu, Y. Pang, X. Zhao, Y. Li, Z. Qin, Z. Liu, P. Lu and X. Bao, *Sensors*, 2022, **22**, 5722.